The American Journal of Human Genetics, Volume *108*

Supplemental information

SPRED2 loss-of-function causes

a recessive Noonan syndrome-like phenotype

Marialetizia Motta, Giulia Fasano, Sina Gredy, Julia Brinkmann, Adeline Alice Bonnard, Pelin Ozlem Simsek-Kiper, Elif Yilmaz Gulec, Leila Essaddam, Gulen Eda Utine, Ingrid Guarnetti Prandi, Martina Venditti, Francesca Pantaleoni, Francesca Clementina Radio, Andrea Ciolfi, Stefania Petrini, Federica Consoli, Cédric Vignal, Denis Hepbasli, Melanie Ullrich, Elke de Boer, Lisenka E.L.M. Vissers, Sami Gritli, Cesare Rossi, Alessandro De Luca, Saayda Ben Becher, Bruce D. Gelb, Bruno Dallapiccola, Antonella Lauri, Giovanni Chillemi, Kai Schuh, Hélène Cavé, Martin Zenker, and Marco Tartaglia

Supplemental Note: Case Reports

Family 1 (c.1142_1143delTT, p.Leu381Hisfs*95)

Subject 1-II-1

The proband, a 14.7-year-old female, is the second child of consanguineous (first cousins) Turkish parents (father, 27 years and mother, 20 years). The family history was positive for a condition overlapping with that observed in the proband (father, father's sister and maternal uncle). Family tree revealed a high degree of inbreeding. The couple had a first pregnancy characterized by premature delivery at 32 weeks of gestation followed by death in the first day; no additional data are available on the clinical presentation of the newborn. The affected father (1-I-1, see below) exhibits short stature, dysmorphic facial features, short and webbed neck, and hypertrophic cardiomyopathy. The proband was born at term by Caesarean section (breech presentation) after a pregnancy complicated with polyhydramnios with a birth weight of 2,000 g. She required hospitalization for 2 weeks for respiratory distress; however, she did not require mechanical ventilation. She had global developmental delay (head control by 2 months, sit with support by 8 months, sit without support by 12 months, and walked after 22 months of age). She presented with language delay (few words with no sentences by 28 months of age). Psychometric evaluation revealed moderate intellectual disability (IQ 50-69) and learning disorder. She attended special education in infancy. A delay in tooth eruption was documented (after 2 years of age). Hip dysplasia was diagnosed in infancy; however, no intervention was performed in the follow-up. She had failure to thrive and a history of recurrent upper and lower respiratory tract infections. She had strabismus, but no intervention had been performed.

Brain MRI revealed mild left cerebral hemisphere enlargement. Echocardiographic evaluation disclosed mild aortic insufficiency, focal interventricular septum hypertrophy, and mitral valve prolapse. She had lymphopenia, with a lymphocyte activation test documented at the lower border of the normal range. T-cell receptor excision circles (TRECs) and naive T cell number were decreased. She received periodic sulfamethoxazole and trimethoprim prophylaxis. Audiologic evaluation and renal ultrasonography were normal. She had easy bruisability without evidence of coagulation defects. No growth hormone deficiency was shown.

At the last evaluation (14.2 years), weight was 42 kg (-1.02 SD), height was 145 cm (-2.41 SD), and head circumference was 57 cm (+1.32 SD). Her craniofacial appearance was characterized by a triangular face, bitemporal narrowing, hypertelorism, mild ptosis, low-set and posteriorly rotated ears with helix folding anomaly and a dysmorphic ear lobe, prominent nasal bridge, low posterior hairline and short/webbed neck. Pectus excavatum and cubitus valgus were also present.

Subject 1-I-1

The affected father is a 40 year-old individual. He has mild intellectual disability but no formal psychometric evaluation had been performed. The educational level was low; learning disabilities were reported. Echocardiographic evaluation revealed class II hypertrophic cardiomyopathy.

At last evaluation (40 years), weight was 56 kg (-1.29 SD), height was 144 cm (-4.35 SD), and head circumference was 56 cm (-1 SD). The craniofacial appearance was characterized by a triangular face, bitemporal narrowing, down-slanted palpebral fissure, low-set and posteriorly rotated ears,

prominent nasal bridge, long philtrum, prominent naso-labial folds, low posterior hairline, and short and webbed neck. Cubitus valgus and mild pectus excavatum were present as well.

Family 2 (c.299T>C, p.Leu100Pro)

Subject 2-II-1

The proband is an 8-year-old boy, second child of apparently healthy, consanguineous (first-degree cousins) Turkish parents. He has two healthy sibs (one brother and one sister) and no affected relative. The family was first referred to our department for genetic counseling because cystic hygroma, polyhydramnios, unilateral ventriculomegaly and renal pelviectasis were identified by ultrasonography (16th week of gestation). The nuchal fold was 8.2 mm. Chromosome analysis of amniocytes showed normal results. He was born on 37th week of gestation with a birth weight of 3,280 g. Neonatal intensive care was required for one week due to late sepsis. On his first examination, he had a coarse face, macrocephaly, wide anterior fontanelle, high forehead, down-slanting palpebral fissures, bilateral epicanthus and hypertelorism, depressed and prominent nasal bridge, low-set posteriorly rotated ears with anterior facing large earlobes, low posterior hairline, webbed neck, wide and short thoracic cage, right cryptorchidism, and loose skin. First echocardiography assessment documented asymmetrical hypertrophy of interventricular septum (7 mm), while trans-fontanelle ultrasonography revealed mild left ventriculomegaly. Diagnosis of Noonan syndrome was posed. *PTPN11* mutation analysis was negative, as well as mutation scan of the other known RASopathy genes.

At follow-up, he showed mild developmental delay (he walked at 19 months), and intellectual disability, and required educational assistance at school. He had atopic complaints with a runny nose and ectodermal problems during infancy (itchy, eczematous skin, dry and scaly skin on face and extensor surfaces of arms and legs). He also had sparse eyebrows and eyelashes with sparse curly and lighter colored hair than his family, loose and thick skin. Immunological tests were normal. He was operated for bilateral nasolacrimal duct stenosis, bilateral exotropia and bilateral cryptorchidism in the first 2 years of his life. He had asymmetrical septal hypertrophy, atrial septal defect (ostium secundum) and pulmonary valvular stenosis. He required pulmonary balloon valvuloplasty (1 year of age). Sharp wave pattern and organization defect on EEG was documented during the second year of his life without occurrence of seizures.

At 2 years of age, brain MRI and control EEG were unremarkable. He had a long aPTT and his coagulation factor XII activity was 24.8%, not requiring treatment. His pectus deformity worsened over time. He had typical pectus carinatum superiorly and pectus excavatum inferiorly; he also had mild pes valgus and planus bilaterally. At 3 and half years, renal ultrasonography revealed grade 2 medullary nephrocalcinosis. His height was between 10th and 25th percentiles, and weight was between 25th and 50th percentiles.

At his last examination, he complained widespread bone pain and myalgia. Laboratory tests were normal. Dysmorphological assessment highlighted an oval face, hypertelorism, downward slanted palpebral fissures, ptosis, prominent glabella, anteverted nares, prominent philtrum, receding chin, low-set ears, folded helix, short webbed neck, pectus carinatum/excavatum, teletelia, kyphosis, and winged shoulder blades.

Family 3 (c.187C>T, p.Arg63*)

Subject 3-II-1

The proband is an 11-year-old Tunisian girl born to consanguineous parents (first-degree cousins). She was referred for a first evaluation at the age of 2.7 years because of splenomegaly. She is the product of an uneventful pregnancy. Delivery occurred by Caesarean section because of macrosomia (birth weight = 4,100 Kg [+2 SD], birth height = 50 cm [0 SD], head circumference = 35.5 cm [+0.5 SD]). Apgar scores were 8, 9, and 10 at 1, 5, and 10 minutes, respectively. The child had moderate pulmonary valve stenosis (30 mmHg), which was discovered at 2 months and confirmed by ultrasound assessment at the age of 2 months and 4 years. The developmental milestones were delayed.

At our first clinical examination, weight was 14 kg (+1 SD), height was 81 cm (-3 SD), and head circumference was 53 cm (+3 SD), with dolichocephaly. A coarse face, relative macrocephaly, high forehead, bitemporal constriction, triangular face, hypertelorism, downslanting palpebral fissures, ptosis of the left eye with convergent strabismus, low-set ears (without posterior rotation and thickening of the ear lobes), prominent nasal bridge, anteverted nostrils, long philtrum, thick lips, high-arched palate with narrow palate, microretrognathia, and pterygium colli with low posterior hairline were noticed. Pectus excavatum with widely-spaced nipples, bilateral clinodactyly of the 4th and 5th fingers, bilateral toe malposition suggestive of diapason-shaped toes, as well as articular hyperlaxity and kyphosis were present. Neurological examination found attention deficit and slight psychomotor delay. Systolic murmur on auscultation was also noted; an ECG and a Holter monitor recording revealed atrial and ventricular extrasystoles. An echocardiogram at age 9.5 years confirmed the moderate pulmonary valve stenosis and revealed moderate mitral regurgitation. Multiple audiograms were normal. Abdominal evaluation revealed splenomegaly reaching the umbilical area without hepatomegaly. Hirsutism of the upper part of the back, and hyperhidrosis were present. Laboratory tests found a mild microcytic hypochromic anemia with normal hemoglobin electrophoresis. A slight increase in serum levels of FT4 with normal levels of TSH.

A follow-up at the age of 9.3 years showed that the proband had skills within lower limits for the age without a defined cognitive deficit. Height was within the normal range while weight was under normal range. She had enuresis and encopresis. Recurrent infections affecting ears (seromucous otitis) and lungs (bronchitis) were reported. The splenomegaly had spontaneously regressed. Chronic constipation was linked to a sigmoid dolichocolon discovered on X-rays.

At our most recent follow-up (11.9 years), height was 136.5 cm (-1.5 SD), weight was 27.5 kg (-2.3 SD), and head circumference was 55cm (+1 SD). She failed her 5th grade school exams.

Karyotype was normal. A diagnosis of Noonan syndrome was suspected, which was not confirmed molecularly.

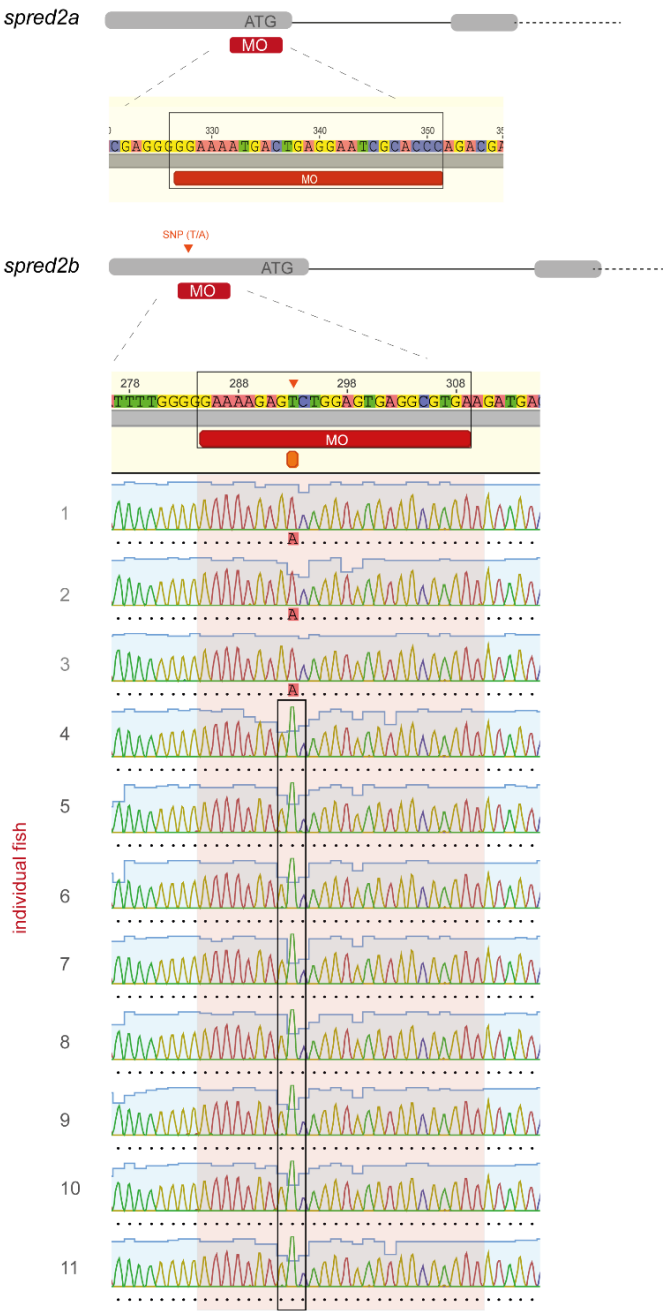

Figure S1. *spred2a* and *spred2b* ATG-MO design and genotyping of the target genomic sequence.

Scheme showing the MO design and target sequence on the 5'-UTR/ATG region of zebrafish *spred2a* and *spred2b* genes. A SNP (T/A) is annotated in the target region of *spred2b* (orange arrowhead). To ensure homogeneous efficiency of the MO-mediated knockdown, Sanger sequencing was performed to select proper genotypes for mating. Chromatograms of the relevant genomic region from individual NHGRI zebrafish embryos are shown in the lower panel. Fish having the "T" allele matching the sequence used to target *spred2b* are outlined by a black line.

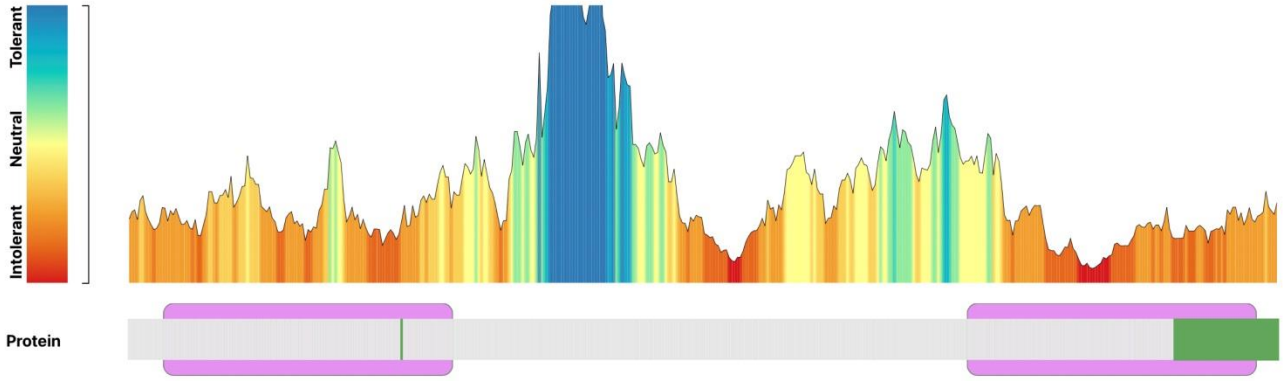

Figure S2. Tolerance landscape of genetic variation for *SPRED2*.

The histograms show the non-synonymous over synonymous (d_N/d_S) ratio for individual residues, as calculated by MetaDome, which are colored according to the scheme reported along the Y-axis. The protein sequence is depicted in grey with the EVH1 (*N*-terminus, left) and SPR (*C*-terminus, right) domains shown in violet. Leu^{100} and the region *C*-terminal to Leu^{381} affected by two of the three homozygous disease-causing variants identified in the study are shown in green. The two pathogenic variants affect two intolerant regions of the protein.

Figure S3. Multiple alignment of the stretches of the EVH1 and SPR domains encompassing Leu^{100} and Leu^{381} of SPRED2 in orthologs and human paralogs.

Position of Leu^{100} and Leu^{381} are indicated (red arrows). The c.1142_1143delTT frameshift at codon 381 was predicted to result in an extended open reading frame characterized by a divergent *C*-terminal tail lacking key residues of the protein required for SPRED2 palmitoylation, a posttranslational modification required for proper targeting of the protein to the plasma membrane. The resulting variant amino acid sequence is above the alignment. Invariant residues among proteins are highlighted in black (consensus > 70%); gray background indicates residues similar to consensus amino acid (grouped as FYW, ILVM, DE, GA, ST, RQ, RKH).

Alignment was generated using MUSCLE v3.8 and visualized by means of pyBoxshade v1.2. SPRED2: *H. sapiens*, NP_861449.2; *M. musculus*, NP_277058.1; *B. Taurus*, XP_005212957.1; *G. gallus*, XP_419341.3; *D. rerio*, NP_998399.1; *X. tropicalis*, NP_001011032.1; *D. melanogaster*, NP_610988.1; SPRED1: *H. sapiens*, NP_689807.1; SPRED3: *H. sapiens*, XP_006723282.1.

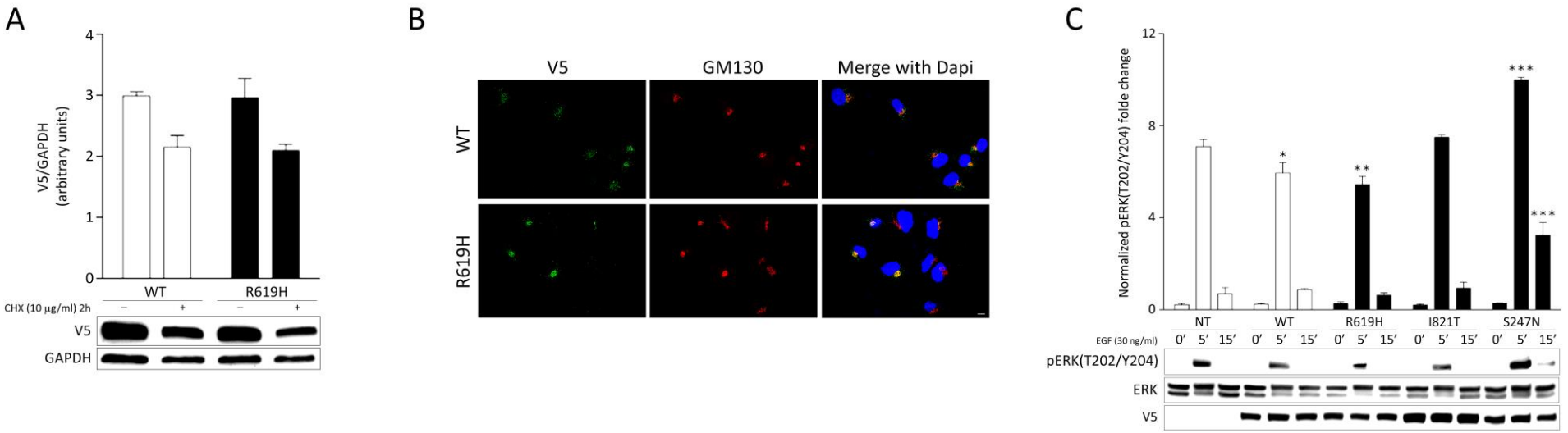

Figure S4. Biochemical and functional characterization of the LZTR1^{Arg619His} protein.

The variant *LZTR1* cDNA was transiently overexpressed in COS-1 cells and tested for stability (A), subcellular localization (B) and impact on pERK levels (C). Previous studies demonstrated that the inactivating *LZTR1* variants implicated in recessive NS cause accelerated degradation or aberrant subcellular localization of LZTR1. When overexpressed, differently from the WT protein, these variants do not downmodulate pERK levels following EGF stimulation. In contrast, dominant negative *LZTR1* variants result in enhanced phosphorylation of ERK following EGF stimulation.

(**A**) Protein levels of the V5-tagged WT and variant (R619H) LZTR1 proteins in transfected COS-1 cells, basally and after CHX (10 µg/mL) treatment. Representative blots and mean ± SD densitometry values of three independent experiments are shown. GAPDH was used as a loading control.

(**B**) Subcellular localization of transiently expressed V5-tagged LZTR1 proteins in COS-1 cells revealed by confocal microscopy analysis. Similar to WT LZTR1, LZTR1^{Arg619His} (R619H) is localized at the level of the Golgi. Cells were stained with the anti-V5 monoclonal antibody (green). Co-localization analysis was performed using the *cis*-Golgi marker GM130 (red). Merged images are shown in the right panels. Scale bar, 10 µm.

(**C**) Similar to the WT protein, LZTR1^{Arg619His} (R619H) weakly but significantly downmodulates ERK phosphorylation when compared with NT (mock transfection) in HEK 293T cells. Overexpression of the recessive NS-causing LZTR1^{Ile821Thr} (I821T) protein fails in modulating ERK phosphorylation, while expression of dominantly acting LZTR1^{Ser247Asn} (S247N) promotes enhanced ERK phosphorylation. Representative blots (below) and mean ± SD densitometry values (above) of three experiments are shown. Asterisks indicate statistically significant differences compared with NT (mock transfection) at the corresponding time upon EGF stimulation (*$P < 0.05$; ** $P < 0.005$; *** $P < 0.001$; two-way ANOVA followed by Tukey's multiple comparison test).

The three assays consistently indicate that the p.Arg619His change does not significantly impact LZTR1 function and MAPK signaling.

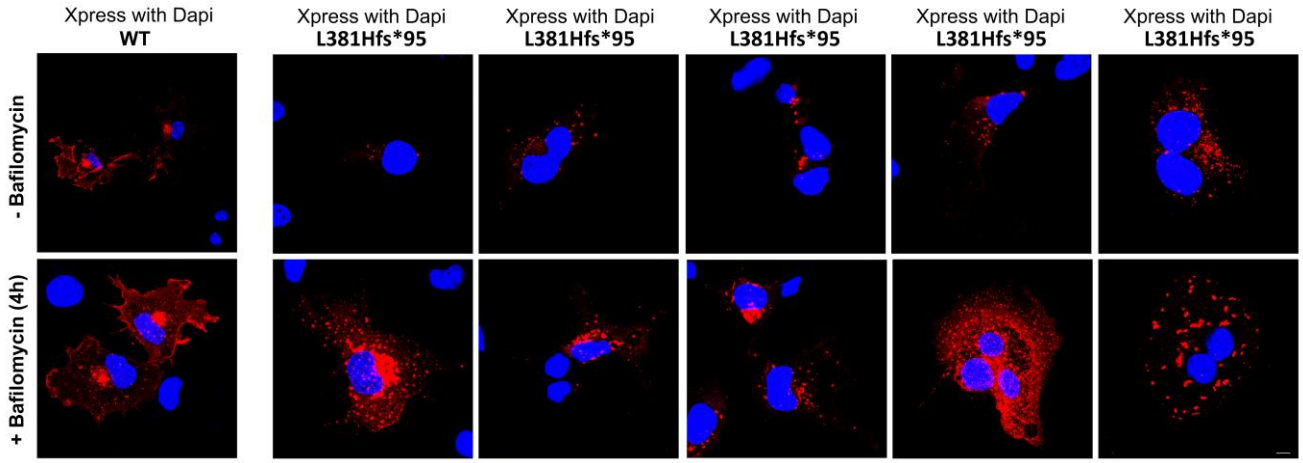

Figure S5. Bafilomycin treatment rescues the accelerated degradation of SPRED2^{Leu381Hisfs*95}.

SPRED2^{Leu381Hisfs*95} (L381Hfs*95) protein accumulates in vesicular structures suggesting its degradation *via* lysosomes. Subcellular localization of transiently expressed Xpress-tagged wild-type and mutated SPRED2 proteins in COS-1 cells under basal conditions and after bafilomycin A1 (200 nM, 4 h) treatment revealed by confocal microscopy analysis. Cells were stained with an anti-Xpress monoclonal antibody and Alexa Fluor 594 goat anti-mouse secondary antibody (red). Merged images with nuclei (DAPI staining, blue) are displayed. Scale bar, 10 μm.

Bafilomycin was used to inhibit autophagy and lysosomal protein degradation (bottom panel). As shown, the treatment resulted in the accumulation of puncta, which likely represent autophagosomes and lysosomes. Differently from the wild-type protein (WT), SPRED2^{Leu381Hisfs*95} does not localize at the plasma membrane.

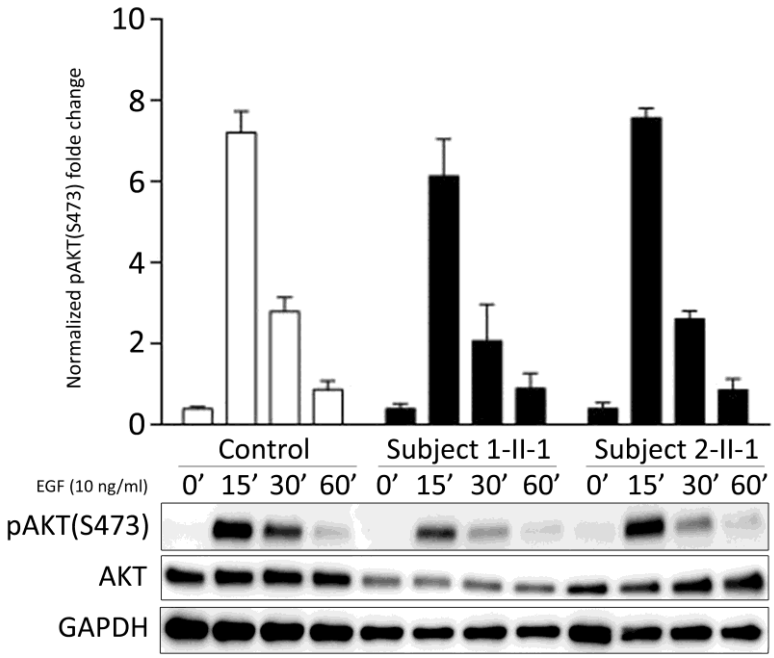

Figure S6. Defective SPRED2 function does not perturb signaling through the PI3K-AKT pathway.

Primary fibroblasts from subjects 1-II-1 (p.Leu381Hisfs*95) and 2-II-1 (p.Leu100Pro) show levels of AKT phosphorylation, basally and after EGF stimulation, that are comparable to those of control cells. Fibroblasts were starved for 16 h and then stimulated with EGF (10 ng/mL), in time-course experiments, or left unstimulated. Equal amounts of cell lysates were resolved on 7.5% polyacrylamide gel. Representative blots (below) and graphs reporting mean ± SD densitometry values (above) of three independent experiments are shown.

These findings are consistent with previous observations indicating that SPRED proteins do not participate in the control of PI3K-AKT signaling.

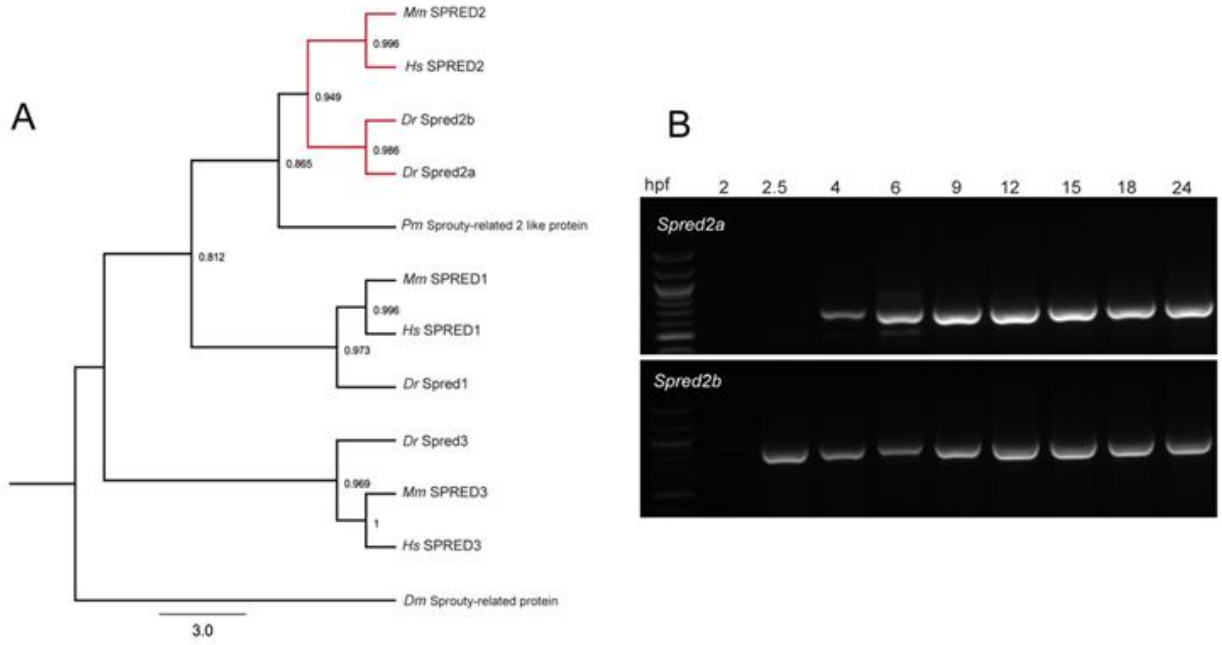

Figure S7. Zebrafish *spred2a* and *spred2b* paralogs, and their expression during early phases of development.

(A) Phylogenetic analysis of the spred2 paralogs (*Dr*, *Danio rerio*) compared to the human (*Hs*, *Homo sapiens*) and mouse (*Mm*, *Mus musculus*) orthologs and paralogs. Sequence data were retrieved from Ensemble. Sequence alignment was generated using Muscle 3.8. Maximum likelihood trees were generated using PhyML 3.0 with the LG substitution model and 100 bootstrap replicates. *Pm*, *Petromyzon marinus*; *Dm*, *Drosophila melanogaster.* Statistical support per node is shown.

(B) RT-PCR showing the expression profile of zebrafish *spred2a* and *spred2b* during early embryogenesis (2-24 hpf, hours post-fertilization).

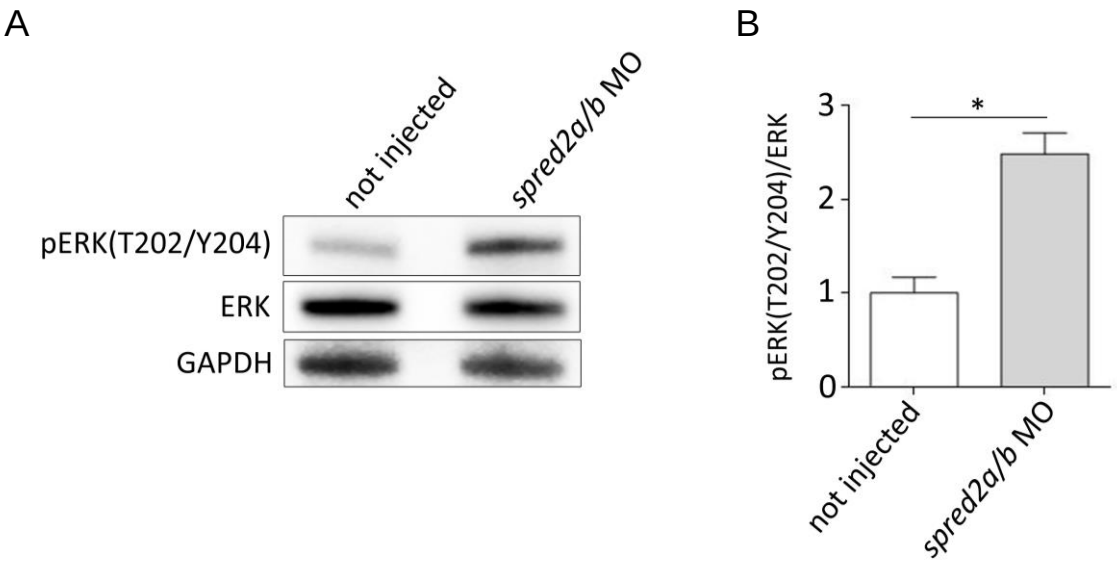

Figure S8. Enhanced Erk phosphorylation in zebrafish embryos injected with *spred2a* and *spred2b* antisense oligonucleotides (MO).

Representative blots (A) and graph reporting mean ± SEM densitometry values (B) of two independent experiments are shown. The asterisk indicates a statistically significant higher Erk phosphorylation level in morphants compared with non-injected embryos (Student's t-test, * indicates $P < 0.05$).

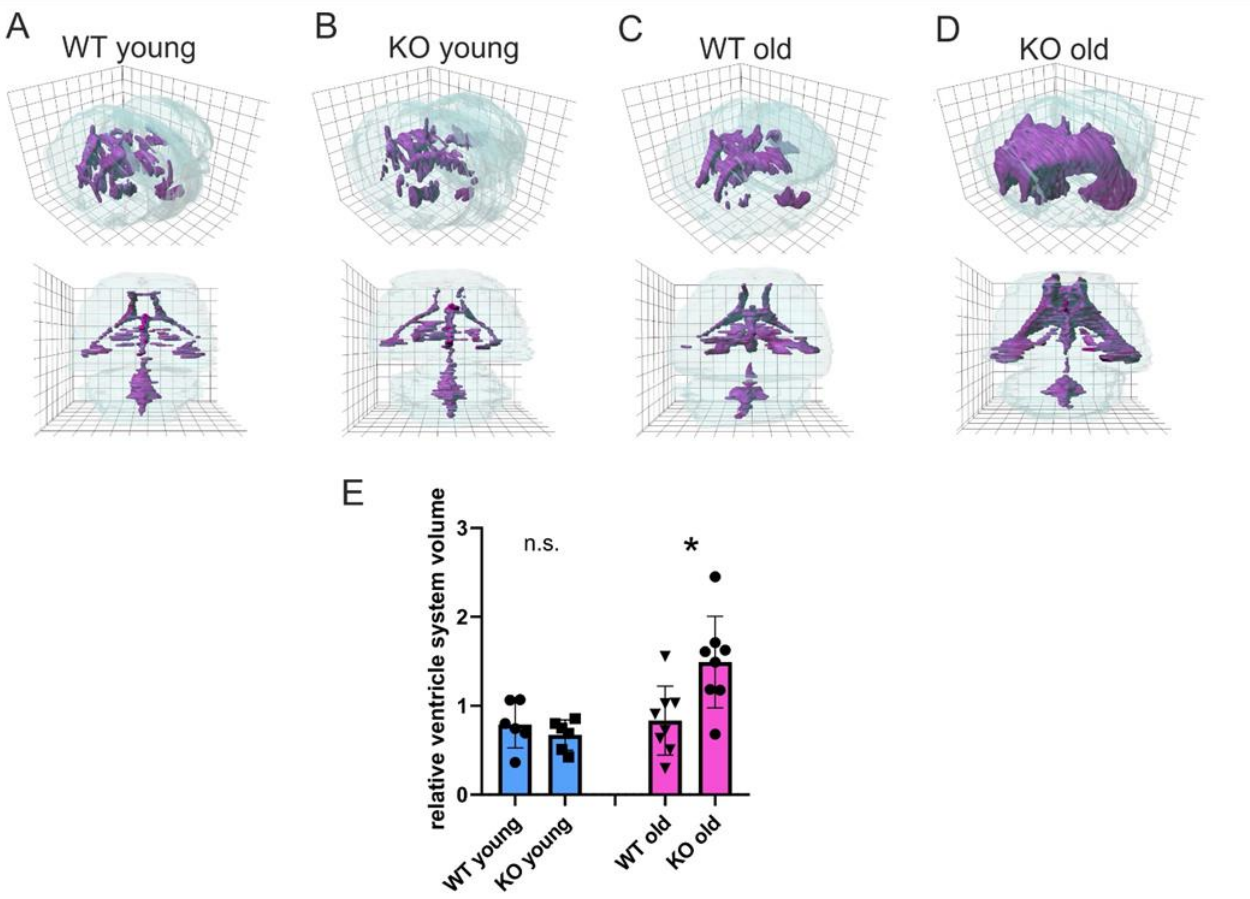

Figure S9. Enlarged brain ventricles in aged *Spred2* KO mice.

(**A**) 3D model of a reconstructed mouse brain ventricular system of a young (6-12 weeks) WT mouse.

(**B**) 3D model of a reconstructed mouse brain ventricular system of a young (6-12 weeks) *Spred2* KO mouse.

(**C**) 3D model of a reconstructed mouse brain ventricular system of an old (12 months) WT mouse.

(**D**) 3D model of a reconstructed mouse brain ventricular system of an old (12 months) *Spred2* KO mouse.

(**E**) Quantification of ventricle system volumes in relation to whole brain volumes (n = 6 in each young group, n = 8 in each old group; * indicates $P < 0.05$).

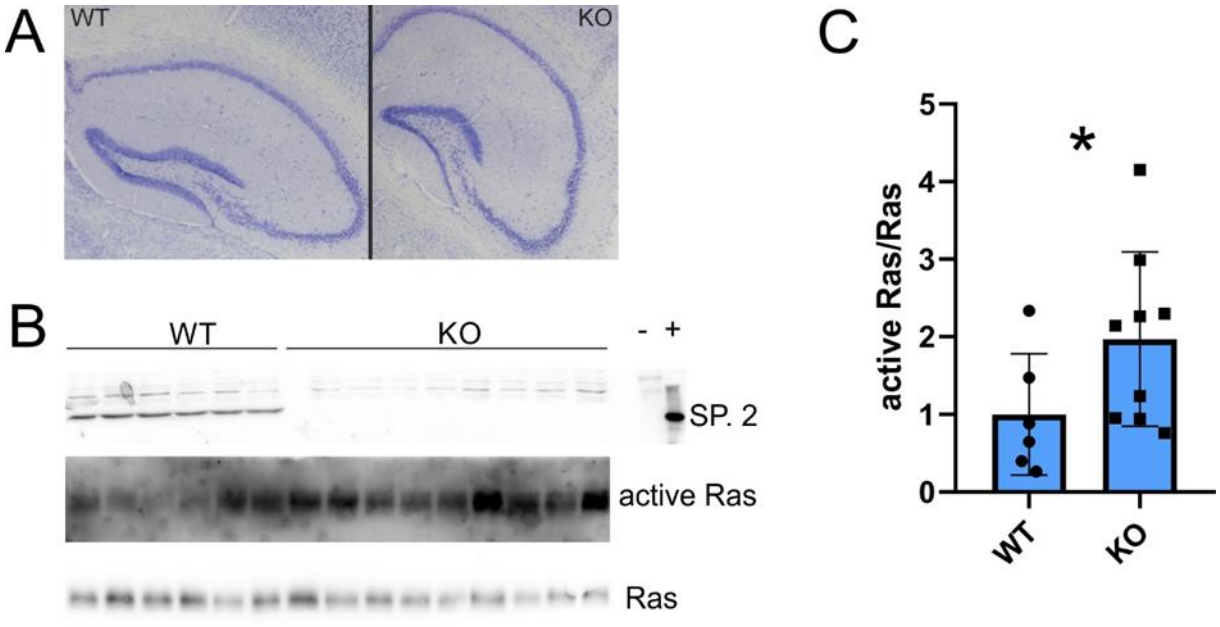

Figure S10. Increased Ras activity in hippocampus of *Spred2* KO mice.

(**A**) Micrographs of Nissl-stained hippocampus regions of a WT mouse in comparison to an age-matched *Spred2* KO mouse. The hippocampus of the KO mice appears compressed and not fully developed, particularly at the structure of the gyrus dentatus.

(**B**) Western blot analysis of hippocampus lysates showing Spred2 levels in WT mice and lack of the protein in *Spred2* KO mice (top). "-" and "+" indicate non-transfected and pCMV-*SPRED2*-transfected HEK 293T cell lysates serving as negative and positive controls, respectively. Middle and lower panels show western blots of pulled-down GTP-bound Ras and levels of total Ras in hippocampus lysates, respectively.

(**C**) Quantification of GTP-bound Ras:total Ras ratio in hippocampus of *Spred2*$^{+/+}$ and *Spred2*$^{-/-}$ mice aged six to twelve months. (WT mice, n = 6; *Spred2* KO mice, n = 9; * indicates $P < 0.05$).

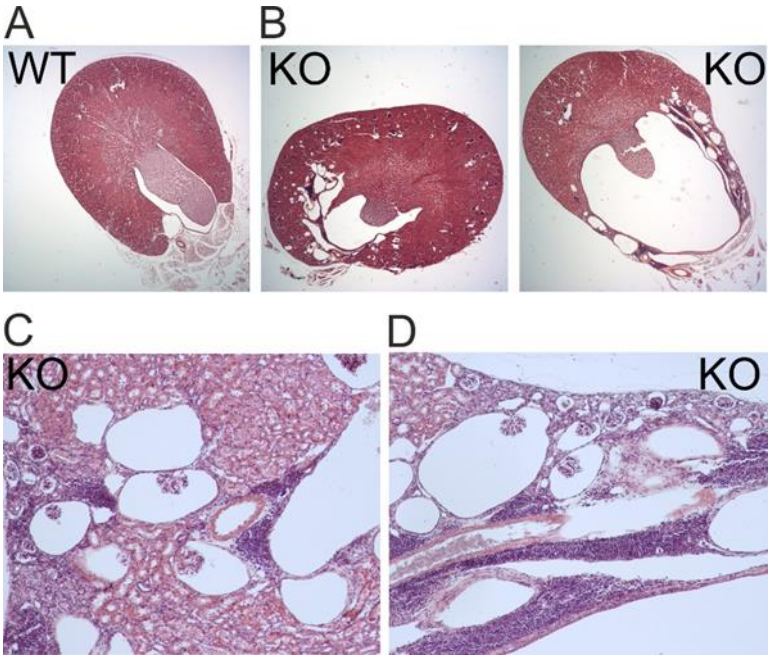

Figure S11. Signs of hydronephrosis and polycystic kidneys in *Spred2* KO mice.

(**A**) Hematoxylin-eosin (HE) stained section of kidney from a WT mouse demonstrating normal structure, no appearance of cysts, and a narrow renal pelvis.

(**B**) Examples of HE stained sections of kidneys from a *Spred2* KO mouse. In these, the renal pelvises were found to be dilated, the renal macroscopic structure was disturbed, and various cysts were visible.

(**C, D**) Higher magnifications revealed multiple cystic formations, expanded Bowman`s capsules, and lymphocyte infiltration in kidneys of *Spred2* KO mice.

Table S1. Clinical features of the disorder caused by SPRED2 LoF compared with neurofibromatosis type 1, Legius syndrome and Noonan syndrome.

Feature	NF1	Legius syndrome	*SPRED2*-related disorder	NS
CALMs	++	++	-	+/-
Freckling	++	++	-	-
Macrocephaly	+	+	+	+
NS-like facial features	+/-	+/-	++	++
Short/webbed neck	+/-	+/-	++	++
Short stature	+/-	+/-	+	++
PVS	+/-	-	+	+
HCM	-	-	+	+
ID	+/-	-	++	+/-
Learning difficulties	++	+	+	+
Lisch nodules	++	-	-	-
neurofibroma	++	-	-	-
Malignant peripheral nerve sheath tumors	+/-	-	-	-
Optic pathway glioma	+	-	-	-
Skeletal defects	sphenoid wing dysplasia, pseudoarthrosis	-	chest defects	chest defects
Inheritance	D	D	R	D/R

D, dominant; R, recessive.